https://doi.org/10.33271/nvngu/2024-3/079

Do Nhu Y[1],
orcid.org/0000-0001-6395-2875,
Trinh Bien Thuy[2],
orcid.org/0009-0006-2427-3515,
Le Anh Tuan[3],
orcid.org/0009-0001-8695-7457,
Ngo Xuan Cuong[*4],
orcid.org/0000-0002-0571-2168

1 – Hanoi University of Mining and Geology, Hanoi, the Socialist Republic of Vietnam
2 – Vietnam–Korea College of Quang Ninh, Ha Long, the Socialist Republic of Vietnam
3 – Hanoi University of Industry, Hanoi, the Socialist Republic of Vietnam
4 – School of Engineering and Technology, Hue University, Thua Thien Hue, the Socialist Republic of Vietnam
* Corresponding author e-mail: ngoxuancuong@hueuni.edu.vn

ROTOR CONFIGURATION FOR IMPROVED WORKING CHARACTERISTICS OF LSPMSM IN MINING APPLICATIONS

Purpose. Analysis of the rotor configuration of line start permanent magnet synchronous motor (LSPMSM) when using 3-bar magnet structure with two cases: one with a separating magnetic steel bridge and one without it. Research results allow selecting the appropriate rotor configuration to obtain the best starting characteristics, current, torque, and performance. Thereby, it is possible to replace high efficiency LSPMSM with low efficiency induction motors used in ventilation and water pumping loads to improve the efficiency of electricity use in mining.

Methodology. The article uses analytical methods and simulation methods on Ansys/Maxwell software and conducts a laboratory test evaluation to determine the effect of rotor configuration on the starting characteristics, working current, torque ripple, and working efficiency of an LSPMSM for mining applications.

Findings. An LSPMSM model was built based on a 15 kW–3,000 rpm induction motor with two rotor configurations: one with a separating magnetic steel bridge and one without it. The results of the study show that when a rotor configuration has no separating magnetic steel bridge, the LSPMSM reaches its maximum speed in 0.45 seconds, a synchronous speed of 3,000 rpm in around 0.75 seconds, a torque ripple of 23.1 %, a current total harmonic distortion of 14.3 %, and a performance of 93.3 %. In contrast, when a rotor structure has a separating magnetic steel bridge, starting the motor is more difficult, taking 1.14 seconds to reach synchronous speed and having a lower starting torque, a current total harmonic distortion of 16.1 %, and a performance of 92.5 %.

Originality. Research rotor configurations of LSPMSM based on the 15 kW–3,000 rpm induction motor with and without a separating magnetic steel bridge. The research results allow choosing the appropriate rotor configuration to obtain the best starting characteristics, current, operating torque and performance efficiency.

Practical value. The research results are important scientific guidance in the design and manufacture of LSPMSM for application in underground mining to improve the efficiency of electricity use in mining.

Keywords: *finite element analysis, asynchronous motor, line start, permanent magnet, rotor configuration*

Introduction. Electricity used in underground mining is mainly used in the technology stages of ventilation, water pumping, transportation, and exploitation, in which the ventilation and water pumping stages account for the largest proportion. 25 to 40 % of a mine's overall energy expenses and 40 to 50 % of its energy usage may be attributed to ventilation systems [1]. Saving energy for mine ventilation fans and water pumps is a necessary issue to reduce the cost of electricity in mining [2–4]. The issue of low-cost energy production is the prospect of sustainable development of the coal mining industry in the world [5].

In Vietnam, ventilation fans and water pumps in underground mining mainly use induction motors (IMs), but IMs often have low efficiency and are difficult to improve the efficiency of the motor [6]. The production of extremely energy-efficient motors has been aided by the fast advancement of rare earth permanent magnet technology with high magnetic field density and the large energy product [7]. Among them, the line-start permanent magnet synchronous motor (LSPMSM) has emerged as an alternative to IM in mine ventilation fans and water pumps [8, 9].

The usage of LSPMSM in industrial constant speed applications is still in its early stages. It is regarded as one of the most promising motor types due to its high efficiency (low CO_2 emissions), high operating power factor, power density, operational torque, low operating temperature, and self-starting capabilities [10]. As a result, LSPMSM is an effective energy-saving solution.

Through the installation of permanent magnets in the IM's rotor, the LSPMSM creates a hybrid between an IM and a synchronous motor. As a result, the LSPMSM can start itself directly and has a high power factor. However, LSPMSM has the disadvantage of having a small starting torque, so it is suitable for blower loads (water pumps) in underground mining [11].

For LSPMSM, although it is confirmed to be a motor with high efficiency and power factor, the most complicated design calculation for LSPMSM is the structural design of the rotor. If the design is not good, the operating parameters may not be guaranteed and may not even meet the standards of IM [12]. In addition, the characteristic of the mining ventilation fan and water pumps is usually a high speed of 3,000 rpm; this is the speed range that is rarely mentioned by research [2].

Several studies have shown that the complexity and influence of the rotor structure in the LSPMSM 3,000 rpm. The paper [13] analyzes the performance of the 2-pole LSPMSM with a rotor structure with three magnets, the magnets are separated by magnetic steel bridges of the rotor. The research results show that with the proposed magnet structure, the motor can achieve IE2 efficiency. In the study [14], the different structure of the electromagnet is studied in the rotor to the starting characteristics of the LSPMSM – based on the IM 37 kW–3,000 rpm prototype motor.

The performance characteristics of the LSPMSM with annular permanent-magnet construction compared to multi-rod rotor structures, all of which are equal to the rotor's magnetic steel bridges, have been studied [15–17]. The research results show that with the annular structure, it will give the best working characteristics, with the performance up to IE3. However, this structure will increase the cost of the magnet and make it difficult to manufacture. In the study [12], the structure of the rotor was optimized by reducing the size of the rotor slot in order to reduce the starting current of the LSPMSM. In the study [18], the author analyzed the working efficiency of LSPMSM with rotor configurations with impeller type to choose the appropriate type of structure to use for the water pump motor.

In the design of the LSPMSM, the starting speed characteristic is often studied first in the operating characteristics, as it confirms the self-starting ability of the motor. In addition, the steady-state operating current characteristics should also be taken into account. Because, for LSPMSM during steady-state operation, the current waveform is usually not "sine" but oscillates harmonically with the supply frequency, thus generating high-order harmonics. This high-order harmonic, if not well controlled, will cause vibration when working for the motor itself [19, 20].

Thus, the structure of the rotor greatly affects the characteristics and working efficiency of the LSPMSM. In the study [21], the LSPMSM rotor with double cage is proposed to improve the synchronization ability of the motor in a wide range as proven by theory. By saving 10 % of the magnet volume, experimental research demonstrates that LSPMSM with a rotor structure that uses both radially magnetized arc shape and circumferentially magnetized spoke shape magnets improves full-load efficiency by 4 % when compared to the benchmarked spoke rotor LSPMSM [22].

To improve motor starting and synchronization, the developed large power LSPMSM includes a hybrid rotor made up of slotted solid steels and cage bars. A conspicuous rotor periphery with air-gap length maximizing at the quadrature axis and minimization at the direct axis is used to lower the harmonics of air-gap flux density and motor losses [23].

Analytical calculations using Matlab for the comparison between four different types of rotor structures (Bar, U-, V- and W-types) of LSPMSM for a constant power speed range have shown that the magnetization direction of the permanent magnet affects the flux distribution and thus controls the flux-weakening behavior, thereby limiting torque and power [24].

For LSPMSMs, the rotor magnetic steel bridges are intended to prevent the path of the magnetic field, which also greatly affects the working efficiency of the motor [25]. Studies on 2-pole LSPMSM mainly analyze and compare different types of magnet structure, while the number of magnetic steel bridges of the rotor also greatly affects the working point of LSPMSM and has not been studied or mentioned.

The research content of the article analyzes the working characteristics of the LSPMSM at 3,000 rpm. In the LSPMSM design, the tooth, slot, magnetic circuit, winding, stator, and rotor squirrel cages remain the same as the corresponding IM, and NdFeB-38 permanent magnets are used. This article will assess the acquired results and make some recommendations for motor production. The configurations are simulated through Ansys/Maxwell software using the finite element method (FEM). In addition, fabrication and laboratory test evaluations were conducted to determine the influence of rotor configuration on the starting characteristics, operating current, torque ripple, and operating performance of the LSPMSM.

The research results provide important scientific guidance in the design and manufacture of high-performance LSPMSM to replace low-performance IMs for important loads such as ventilation and water pumping, thereby improving the efficiency of electricity use in mining, actively contributing to sustainable development in the mining industry.

Mathematical model of LSPMSM. Mathematical model of LSPMSM is written in d, q coordinate system with input parameters being applied as follows [26, 27].

Stator and rotor voltage equations

$$\begin{cases} u_{ds} = r_1 i_{ds} + \dfrac{d\psi_{ds}}{dt} - \omega_r \cdot \psi_{qs} \\ u_{qs} = r_1 i_{qs} + \dfrac{d\psi_{qs}}{dt} + \omega_r \cdot \psi_{ds} \end{cases}; \quad (1)$$

$$\begin{cases} u'_{dr} = r'_{dr} i'_{dr} + \dfrac{d\psi'_{dr}}{dt} = 0 \\ u'_{qr} = r'_{qr} i'_{qr} + \dfrac{d\psi'_{qr}}{dt} = 0 \end{cases}. \quad (2)$$

The stator and rotor flux equations are

$$\begin{cases} \psi_{ds} = (L_{ls} + L_{md}) i_{ds} + L_{md} \cdot i'_{dr} + \psi'_m \\ \psi_{qs} = (L_{ls} + L_{md}) i_{qs} + L_{mq} \cdot i'_{qr} \end{cases}; \quad (3)$$

$$\begin{cases} \psi'_{dr} = L'_{lr} i'_{dr} + L_{md}(i_{ds} + i'_{dr}) + \psi'_m \\ \psi'_{qr} = L'_{lr} i'_{qr} + L_{mq}(i_{qs} + i'_{qr}) \end{cases}, \quad (4)$$

where ω_r is rotor angular speed; Ψ'_m – stator loop flux produced by permanent magnets; L_{ls} – stator winding dissipation inductance; L_{md} – axial synchronous magnetizing inductance; L_{mq} – horizontal synchronous magnetizing inductance; i_{ds} – axial stator current component; i_{qs} – horizontal stator current component; i'_{dr} – axial converted rotor current component; i'_{qr} – axial converted rotor current component.

According to the mathematical description equations (1–4), *d-axis* and *q-axis* equivalent circuit diagram of LSPMSM has been built to satisfy the voltage and flux equations in the mathematical model in Figs. 1 and 2, in which to model instead $\Psi'_m = L_{rc} \cdot i'_m$, L_{rc} is the fictitious reactance of a permanent magnet; i'_m is the equivalent magnetization current converted to the stator of the permanent magnet [26, 27].

The electromagnetic torque of the LSPMSM is determined

$$M = \frac{3}{2} p[(L_{md} \cdot i'_{dr} \cdot i_{qs} - L_{mq} \cdot i'_{qr} \cdot i_{ds}) + \Psi'_m \cdot i_{ds} + (L_{md} - L_{mq}) i_{ds} \cdot i_{qs}] = M_{asyn} + M_{\text{exc}} + M_{rel}, \quad (5)$$

where M_{asyn} is asynchronous torque component; M_{exc} – excitation torque component; M_{rel} – reluctance torque component.

From the electromagnetic torque equation can be seen, the electromagnetic torque of the LSPMSM consists of the excitation torque components, the reluctance torque will be equivalent to that of a permanent magnet synchronous motor. LSPMSM only has an additional asynchronous torque component and this component plays a decisive role in the starting ability of the motor [27].

Research on rotor structure of LSPMSM. The typical LSPMSM is based on the IM 15 kW–3,000 rpm motor prototype used for the mine ventilation fan. The tooth structure, slot, magnetic circuit, windings, stator, and rotor squirrel cages remain the same, according to IM. The parameters of the LSPMSM are given in Table 1 [15].

The experimental configuration of the 3-phase LSPMSM 15 kW–3,000 rpm with voltage 380/660 V is as shown in Fig. 3,

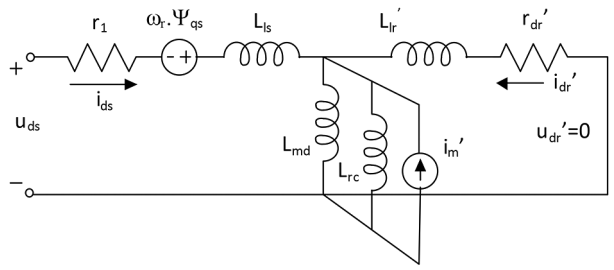

Fig. 1. d-axis equivalent circuit diagram of LSPMSM

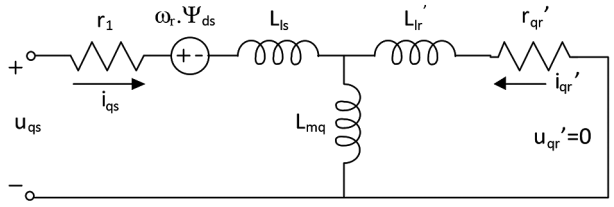

Fig. 2. q-axis equivalent circuit diagram of LSPMSM

Table 1

Parameters of the LSPMSM

Parameters	Symbol	Value	Unit
Stator Outer Diameter	D_{in}	245	mm
Stator inner diameter	D_{out}	152	mm
Rotor outer diameter	D'	151	mm
Rotor shaft diameter	D_t	52	mm
Stator steel material	Steel 1008		
Number of stator slots	Z_1	36	slots
Number of rotor slots	Z_2	28	slots
Air gap length	g	0.5	mm
Power supply voltage	U_n	380/660	V
Power supply frequency	f	50	Hz

in which the dimensions of the permanent magnet have corresponding values of thickness *h* (mm) and width *b* (mm).

The permanent magnet structure used to fabricate the research LSPMSM is a 3-bar magnet structure, using NdFeB-38 magnets with a size of ($b.h = 35 \cdot 9$ mm) each. Permanent magnets NdFeB-38 is a type of permanent magnet made from an alloy of neodymium, iron and boron. They are used in many different applications. NdFeB magnets continue to be the strongest permanent magnets marketed due to their high energy storage capacity compared to Fe, AlNiCo or SmCo permanent magnets [28].

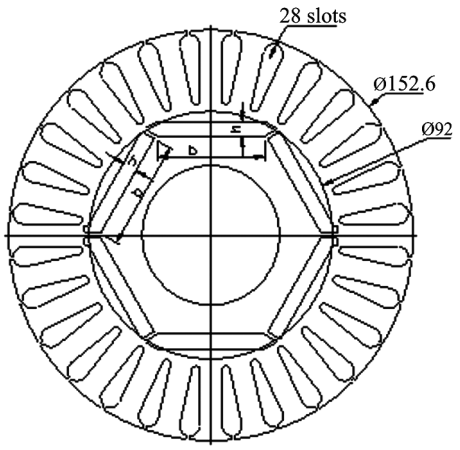

Fig. 3. Rotor configuration of the proposed LSPMSM

The magnet bars in LSPMSM – 3000 rpm can be separated from each other by the magnetic steel edges of the rotor called a magnetic bridge (Fig. 4, *a*) or without magnetic bridges, as shown in Fig. 4, *b*. The use of magnetic bridges (Fig. 4, *a*) facilitates the installation of magnets, helps the magnet bar to be fixed better, and the structure of the rotor is more solid. However, using these magnetic bridges leads to the appearance of many stray magnetic fields in the rotor magnetic circuit, which can worsen the working characteristics and performance of the motor; in addition, the manufacturing cost of making the magnet grooves increases. Not using magnetic bridges (Fig. 4, *b*) has the advantage of reducing the manufacturing cost of making magnet tracks and reducing the motor's stray magnetic field, which can improve working characteristics. Thus, the arrangement or not to arrange magnetic bridges to separate the magnet bars is also an issue that needs to be resolved to improve the working characteristics of the LSPMSM – 3000 rpm.

Finite element method through Ansys/Maxwell software is used to analyze rotor structure in two cases. The solution to the Poisson equation for the electromagnetic field of the electric motor model is the distribution of the magnetic field in the magnetic circuit and the surrounding area of the electromagnetic structure. The foundation of this model is Maxwell-Ampere's law. The Maxwell-Faraday equation, which is expressed as follows for the case of a steady-state electric motor, states [8, 12]

$$\nabla \cdot \vec{H} = \vec{J}, \tag{6}$$

where $\vec{J}$ is the density of direct current in the electromagnet coil, A/m^2; $\vec{H}$ – magnetic field strength, H/m.

The magnetic flux density $\vec{B}$ and the magnetic field strength $\vec{H}$ are related in the following way

$$\vec{B} = \mu_0 \cdot \mu_r \cdot \vec{H}, \tag{7}$$

where μ_0 is magnetic permeability of vacuum; μ_r – relative permeability of magnetic conducting environment.

The magnetic potential vector $\vec{A}$ in the electromagnetic field is used to calculate the magnetic flux density $\vec{B}$, as follows

$$\vec{B} = \nabla \cdot \vec{A}. \tag{8}$$

The equation that results from replacing (7 and 8) in equation (6) is as follows

$$\nabla \times \left(\frac{1}{\mu_0 \cdot \mu_r} \nabla \cdot \vec{A} \right) = \vec{J}. \tag{9}$$

Poisson's equation, which has the general form given by equation (9), can be understood as follows in the analytical model corresponding to the Oxyz coordinate system

$$\frac{1}{\mu_0 \cdot \mu_r} \left(\frac{\partial^2 A}{\partial x^2} + \frac{\partial^2 A}{\partial y^2} + \frac{\partial^2 A}{\partial z^2} \right) + J = 0. \tag{10}$$

The magnetic potential vector $\vec{A}$ can be found through (10). Utilizing the solutions to equations (7 and 8) compute the magnetic flux density $\vec{B}$ and magnetic field intensity $\vec{H}$ as follows

$$\vec{B} = B_x \cdot \vec{i} + B_y \cdot \vec{j} + B_z \cdot \vec{k} =$$
$$= \left(\frac{\partial A_z}{\partial y} - \frac{\partial A_y}{\partial z} \right) \vec{i} + \left(\frac{\partial A_x}{\partial z} - \frac{\partial A_z}{\partial x} \right) \vec{j} + \left(\frac{\partial A_y}{\partial x} - \frac{\partial A_x}{\partial y} \right) \vec{k}.$$

The following equations can be used to calculate the DC current of the coil and the voltage applied to its two coil terminals

$$U = R_{dc} i + L \frac{di}{dt}; \quad I_{dc} = \frac{U}{R_{dc}},$$

where U is voltage applied to the two coil terminals; R_{dc} – DC resistance of the coil; L – inductance of the coil; I_{dc} – current in the coil.

The finite element method is a technique to solve (10) to determine the magnetic potential vector A. Through that, magnetic induction B and magnetic field intensity H in equations (6 and 7) are calculated, thereby determining the magnetic field distribution in space with high accuracy. This will be very beneficial to the designers and operators of the magnetic sorting machine when they are modifying the electromagnetic structure's parameters in order to optimize the distribution of magnetic fields in space and raise the machine's operational efficiency. The four fundamental steps of the FEM method are as follows [13]:

1. Divide the domain of analysis into discrete elements. The elements are joined to create a mesh.

2. Select a membership function, then get a rough answer for every element.

3. Combine all elements in the analysis domain to obtain the system matrix.

4. Utilize an iterative approach to solve the system matrix.

In order to do calculations with the finite element approach, digital computers and software applications built on the mathematical underpinnings of FEM are required.

In the first case, the rotor magnetic steel bridges are used to separate the permanent magnet rods, and in the second case, there is no separating magnetic steel bridge between the rods, as shown in Fig. 4.

Research results:

1. Magnetic field distribution. The magnetic field distribution in the LSPMSM is the overall picture to evaluate the use of permanent magnets and the magnetic flux distribution in the motor (Fig. 5).

Surveying the distribution of magnetic field paths (Fig. 5) using Ansys/Maxwell software has shown that in the case with a separating magnetic steel bridge, more closed-loop stray magnetic fields appear in the rotor's magnetic circuit than in the case without a separating magnetic steel bridge. This reduces the amount of magnetic field generated by the NdFeB-38 permanent magnet and does not close the loop with the stator coil, leading to reduced performance and working characteristics of LSPMSM.

2. Starting characteristics of the motor. Starting characteristics of the motor are shown in Fig. 6.

From Fig. 6, for the two study structures, all LSPMSMs can reach rated speed. However, the starting speed characteristic of the LSPMSM with the bridgeless rotor configuration is better. In the case of a rotor structure without a separating magnetic steel bridge, the motor reaches the maximum speed after 0.45 s; besides, after about 0.75 s, the motor reaches a synchronous speed of 3,000 rpm. In the case of a rotor structure with a separating magnetic steel bridge, starting the motor is more difficult, and the time for the motor to reach synchronous speed is 1.14 s.

The quick start of the LSPMSM is well suited to explosion-proof mine ventilation fans, which help quickly reduce the amount of dust in mines, ensuring safety in mining.

3. Torque characteristics of the motor. The torque characteristics of the motor are given in Fig. 7.

The results of the study show that, in the case of a rotor structure without a separating magnetic steel bridge, the motor has a larger starting torque than in the case of a rotor structure with a separating magnetic steel bridge. Thus, in the case of a rotor structure without a separating magnetic steel bridge, the motor works with less vibration.

Simulation results allow analyzing the starting parameters of the motor: time to reach synchronous speed (t_s), transient time (t_{trans}), speed (ω), maximum torque (M_{max}) and Torque ripple ($RipT$). Torque ripple of LSPMSM can be calculated [29]

$$RipT = \frac{T_{\max} - T_{\min}}{T_e},$$

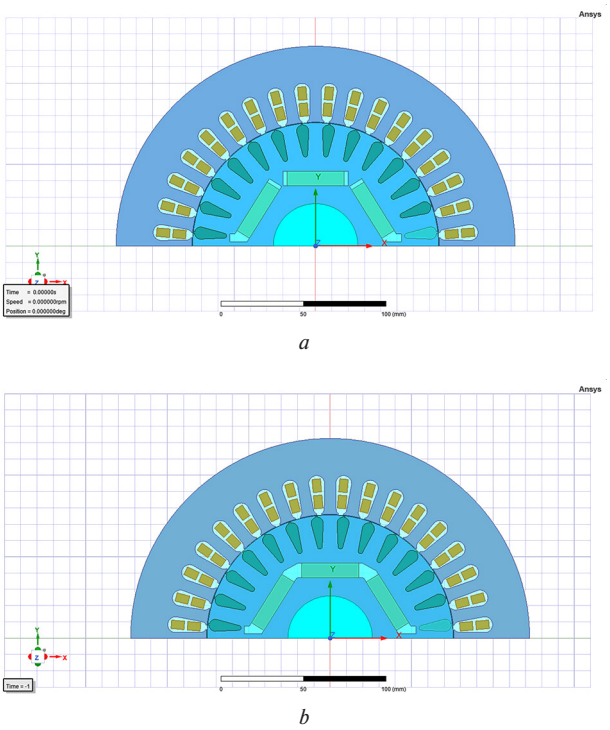

a

b

Fig. 4. Structure of the rotor:

a – with separating magnetic steel bridge; b – without separating magnetic steel bridge

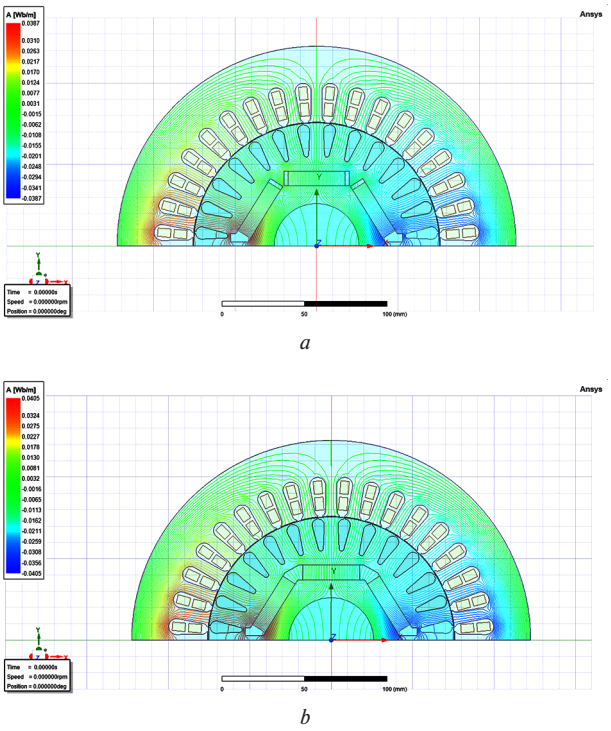

a

b

Fig. 5. Magnetic field distribution in the motor:

a – with a separating magnetic steel bridge; b – without a separating magnetic steel bridge

where $T_{\max}$ is maximum torque value; $T_{\min}$ – minimum torque value; T_e – average torque value of electric motor, N · m; R_{ipT} – torque ripple, %.

From the results on the startup characteristics in Figs. 6, 7, and Table 2 in the case of a rotor structure without a separating magnetic steel bridge, there is reached synchronous speed (t_s = = 0.45 s), transient time (t_{trans} = 0.75 s),) and Torque ripple ($RipT$ = 23.1 %). While the case with a separating magnetic

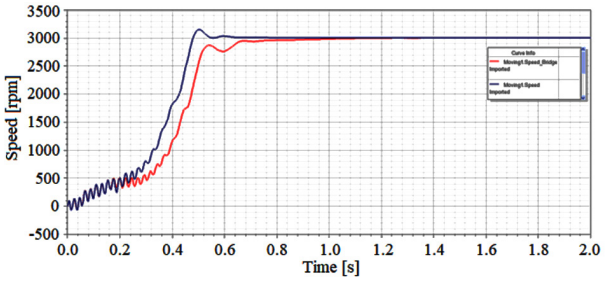

Fig. 6. Starting characteristics of the motor

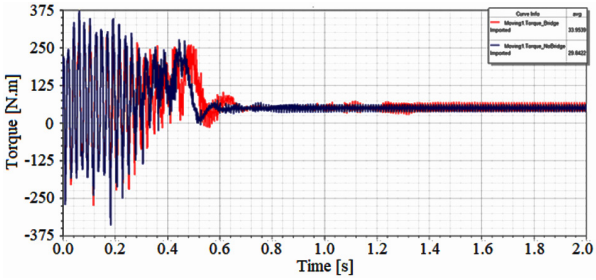

Fig. 7. Torque characteristics of the motor

Table 2

Torque characteristics of the motor

Type	t_s (s)	t_{trans} (s)	*RipT* (%)
Without a separating magnetic steel bridge	0.45	0.75	23.1
With a separating magnetic steel bridge	1.14	1.14	26.6

steel bridge has parameters synchronous speed (t_s = 1.14 s), transient time (t_{trans} = 1.14 s),) and torque ripple (*RipT* = = 26.6 %). Thus, it can be seen that not using a bridge will make the LSPMSM have better working characteristics than when using magnetic bridges.

4. Current characteristics. The current characteristics of LSPMSM in steady-state operating mode are shown in Fig. 8.

Fig. 8 shows that all of the LSPMSM's current characteristic waveforms in steady-state mode, regardless of configuration, are non-sine. The current waveform will oscillate at a frequency of 50 Hz.

The analysis of the harmonic spectrum components of the current in the LSPMSM is shown in Fig. 9. It can be seen that the *3rd* harmonic amplitude in the case of a rotor structure separating magnetic steel bridge reaches nearly 6 A, and in the case of a rotor structure separating magnetic steel bridge it reaches nearly 4 A. Such as, the current waveform in the case of a rotor structure without a separating magnetic steel bridge will be in a form closer to sine than in the case of a rotor structure with a separating magnetic steel bridge.

The simulation results show that the current is distorted so the current includes many harmonic components. Current to-

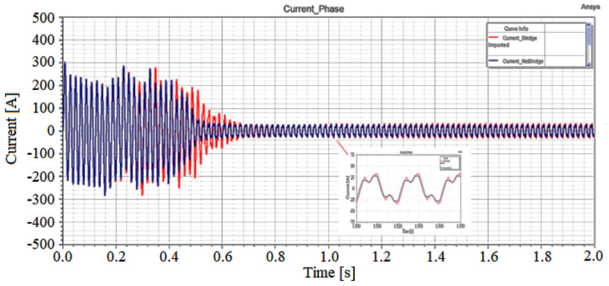

Fig. 8. Current characteristics in steady-state operating mode

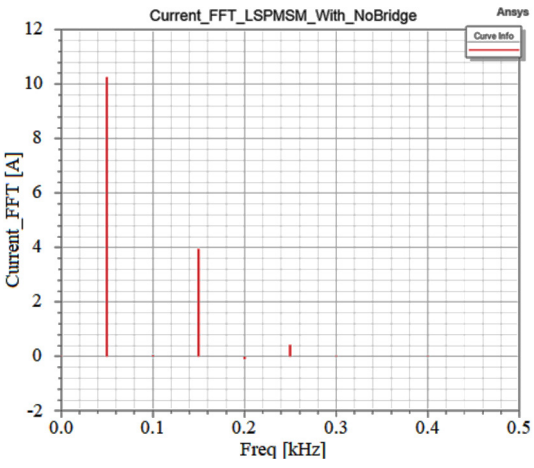

a

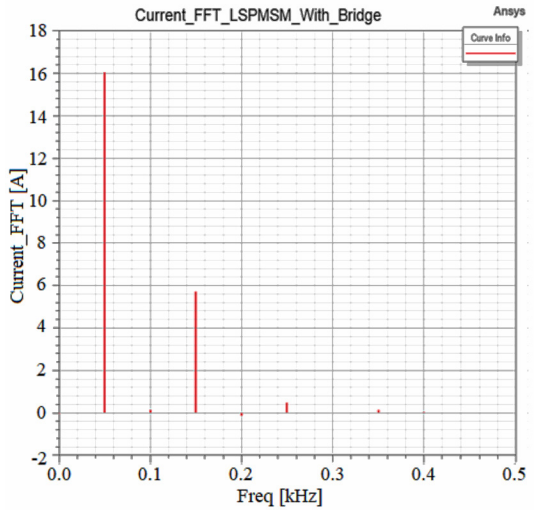

b

Fig. 9. Analysis of current harmonic spectrum:

a – without separating magnetic steel bridge; b – with separating magnetic steel bridge

tal harmonic distortion (THD) can be computed using the formula below [30, 31]

$$THD_i = \frac{\sqrt{\sum_{n=2}^{\infty} I_n^2}}{I_1}.$$

From the analysis results in Figs. 8, 9 and Table 3, it is shown that in the case of the rotor configurations without a separating magnetic steel bridge, the current characteristic has a current transient time t_{trans} = 0.8 s, maximum current I_{max} = = 312 A, and total harmonic distortion THD_i = 14.3 %. In the case of the rotor configurations with a separating magnetic steel bridge the current characteristic has a current transient time t_{trans} = 0.95 s, maximum current I_{max} = 314 A, and total harmonic distortion THD_i = 16.1 %. Thus, in the case of rotor configurations without a separating magnetic steel bridge LSPMSM will have better characteristics.

Table 3

Current characteristics of the motor

Type	t_{trans} (s)	I_{max} (A)	THD_i (%)
Without a separating magnetic steel bridge	0.80	312	14.3
With a separating magnetic steel bridge	0.95	314	16.1

5. The electromotive force (EMF) characteristics. The EMF characteristics in Fig. 10 are the output voltage characteristics of the stator coil when LSPMSM works in generator mode.

The results given in Fig. 10 show that in both investigated cases, the EMF characteristics are sinusoidal and similar. However, in the case of using a magnetic bridge, the EMF characteristics has a larger fluctuation amplitude than when not using a magnetic bridge. To evaluate the degree of difference of the no-load output voltage compared to the rated value, use the formula [32]

$$\Delta E\% = \frac{E_{1NB} - 380}{E_{1NB}} 100\,\%,$$

where E_{1NB} is the RMS value of the I^{st} harmonic of the no-load output voltage.

The calculation results show that difference of the no-load output voltage in the case of the rotor configurations without a separating magnetic steel bridge $\Delta E = 2.3\,\%$, in the case of the rotor configurations with a separating magnetic steel bridge $\Delta E = 5.1\,\%$. Thus, difference of the EMF characteristics in the case of the rotor configurations without a separating magnetic steel bridge is better.

6. Electromagnetic power and mechanical power. Characteristics of electromagnetic power and mechanical power to calculate motor efficiency during simulation are given in Fig. 11.

Based on the electromagnetic characteristics and mechanical power calculate the performance of LSPMSM, in the case of the rotor configurations without a separating magnetic steel bridge, the efficiency is $\eta = 93.3\,\%$, in the case of the rotor configurations with a separating magnetic steel bridge, the efficiency is $\eta = 92.5\,\%$.

Thus, research and evaluation of speed characteristics, torque characteristics, current characteristics, EMF characteristics and performance of LSPMSM using finite element method based on Ansys/Maxwell simulation software showed that the rotor configurations without a separating magnetic steel bridge allows the LSPMSM to have better working parameters. This structure is used for manufacturing and experimental evaluation.

Experimental research in the laboratory. The experimental evaluation was conducted at the Department of Electrification, Hanoi University of Mining and Geology. The rotor groove structure is fabricated as the structure selected by analysis, then the NdFeB-38 magnet is installed and completed as shown in the illustration of element number *6* in Fig. 12.

After completing the rotor, we completely assemble the LSPMSM and complete the experimental diagram of the working parameters of motor. Measurement of the characteristics of the experimental LSPMSM will be performed by coupling the motor to a computer via the NI Card USB-6009. Speed characteristics are measured through Encoder, current characteristics are measured through current transformer as shown in Fig. 12.

The results of investigating the current characteristics of the LSPMSM on the oscilloscope with the laboratory test model are given in Fig. 13.

The results in Fig. 13 show that the current characteristics have a sinusoidal shape, with a shape like the current shape as shown in the simulation results given in Fig. 8. In addition, seeing that the harmonic level of the current is quite large, analyzing the total harmonic content on the osilocop gives the result $THD_i = 14.9\,\%$, like the simulation results as shown in Table 3.

Investigation of the EMF characteristics of the LSPMSM is given in Fig. 14.

The EMF measurement results in Fig. 14 show that the EMF characteristics have a sinusoidal shape. The measured value of 379 V differs from the rated value of 1 V (equivalent to $\Delta E = 0.2\,\%$), completely equivalent to the simulation results shown in Fig. 10.

With the load parameters changing from 0–110 % of the rated load, and with the conversion efficiency of the mechanical coupling mechanism and generator being 82 %, the performance characteristics of the LSPMSM motor are given in Fig. 15.

The results in Fig. 15 show that the motor's efficiency reaches a maximum of 92.5 % at a load level of about 92 % of the rated load. When the motor load exceeds 100 % of the rated load, the motor performance tends to gradually decrease. This result is lower than the performance level shown in the simulation results due to technological error factors in the manufacturing process of LSPMSM.

The studied motor has a power of 15 kW, a speed of 3,000 rpm, and a voltage of 380/660 volts. This is a small power motor and the most used motor for local ventilation fans and local water pumps in mining in Vietnam. Therefore, the motor with the proposed rotor structure will be applied in practice for loads such as local ventilation fans and local water pumps in mining.

Currently, for the mine's main drainage pump or main fan, motors with a large power of hundreds of kW and a high voltage of 6 kV are used. To apply the research on these motors, it is necessary to continue research and evaluation using

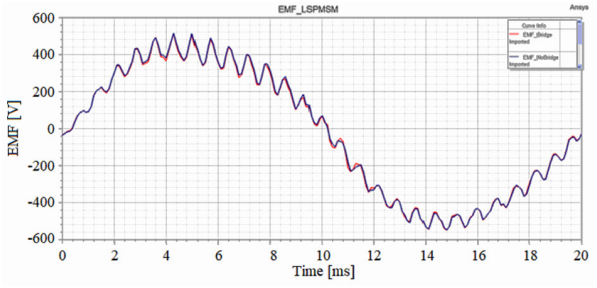

Fig. 10. EMF characteristics

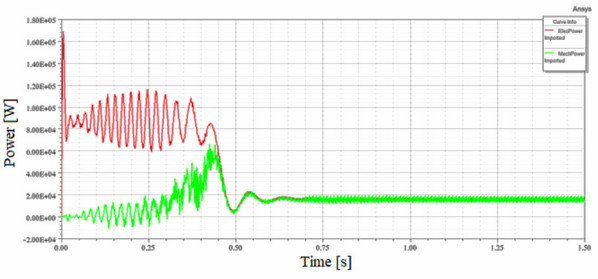

Fig. 11. Electromagnetic power and mechanical power during LSPMSM simulation

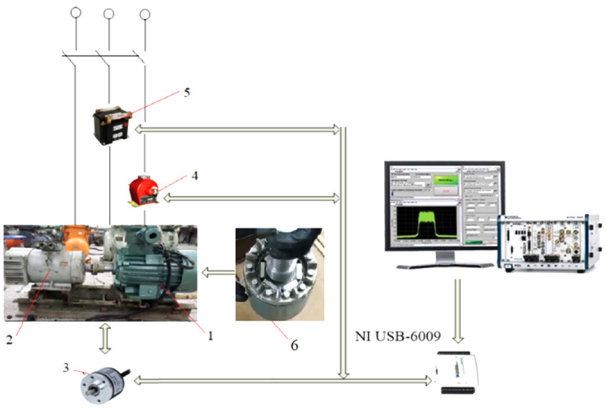

Fig. 12. Laboratory test model:
1 – LSPMSM; 2 – Generator; 3 – Encoder; 4 – CT current transformer; 5 – Transformer; 6 – Fabricated rotor structure

Fig. 13. Current characteristics of the LSPMSM on the oscilloscope

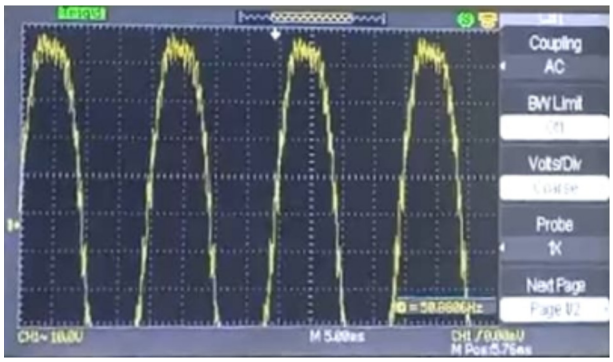

Fig. 14. EMF measurement results of LSPMSM

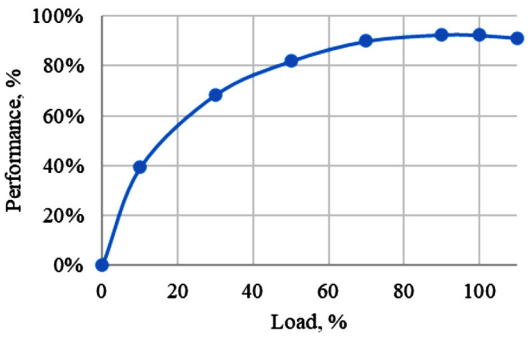

Fig. 15. Performance characteristics of LSPMSM

theory and experiment before implementing testing in practice. This is also one of the next research directions.

Conclusions. The article presented a mathematical model for LSPMSM through simulation and experimentation to determine the effect of rotor configuration on the working characteristics of LSPMSM for mining applications.

An LSPMSM model was built based on a 15 kW–3,000 rpm induction motor with two rotor configurations: one with a separating magnetic steel bridge and one without it. The results of the study show that when a rotor configuration has no separating magnetic steel bridge, the LSPMSM reaches its maximum speed in 0.45 s, a synchronous speed of 3,000 rpm in around 0.75 s, a torque ripple of 23.1 %, a current total harmonic distortion of 14.3 % and a performance of 93.3 %. In contrast, when a rotor structure has a separating magnetic steel bridge, starting the motor is more difficult, taking 1.14 seconds to reach synchronous speed and having a lower starting torque, a current total harmonic distortion of 16.1 %, and a performance of 92.5 %. Experimental results on rotor configuration with separating magnetic steel bridges have shown similar results with simulations. Specifically, the proposed LSPMSM has a current total harmonic distortion of 14.9 %, the EMF has a sinusoidal shape, and the motor's efficiency reaches a maximum of 92.5 % at a load level of about 92 % of the rated load.

The research results show that in the case of a rotor structure without a separating magnetic steel bridge, the LSPMSM has the best starting speed and steady-state current characteristics. And in this case, the LSPMSM has the fastest starting speed, low oscillation operating torque, and near-sine steady-state operating current characteristics. With this configuration, the fabrication of LSPMSM will also become more convenient, and this will be the configuration chosen in actual manufacturing for mining applications in the near future.

Acknowledgments. *This work was partially supported by: 1. Hanoi University of Mining and Geology; 2. Hue University under the Core Research Program, Grant No. NCTB. DHH.2024.08.*

References.

1. De Souza, E. (2015). Improving the energy efficiency of mine fan assemblages. *Applied Thermal Engineering*, *90*, 1092-1097. https://doi.org/10.1016/j.applthermaleng.2015.04.048.

2. Babu, V., Maity, T., & Prasad, H. (2015). Energy saving techniques for ventilation fans used in underground coal mines – A survey. *Journal of Mining Science*, *51*, 1001-1008. https://doi.org/10.1134/S1062739115050198.

3. Pitis, C., & Livingstone, A. (2004). Energy efficient fans in underground auxiliary ventilation systems. *1st ICUE International Conference of Industrial and Commercial Use of Energy Proceedings, Cape Town*. 103.

4. Yu, B. C., & Shao, L. S. (2022). A Mine Ventilation System Energy Saving Technique Based on an Improved Equilibrium Optimizer. *Frontiers in Energy Research*, *10*, 913817. https://doi.org/10.3389/fenrg.2022.913817.

5. Zhironkin, S., & Cehlár, M. (2021). Coal mining sustainable development: economics and technological Outlook. *Energies, 14*(16), 5029. https://doi.org/10.3390/en14165029.

6. Zhou, P., Xu, Y., & Zhang, W. (2023). Design Consideration on a Low-Cost Permanent Magnetization Remanufacturing Method for Low-Efficiency Induction Motors. *Energies*, *16*(17), 6142. https://doi.org/10.3390/en16176142.

7. Do, T. D., Do, Y. N., & Dai, P. D. (2018). A robust suboptimal control system design of chaotic PMSMs. *Electrical Engineering*, *100*(3), 1455-1466. https://doi.org/10.1007/s00202-017-0603-6.

8. Do, N. Y., Do, A. T., Le, A. T., & Luu, V. U. (2022). Design of high-performance explosion proof motor of 3,000 rpm for local exhaust ventilation in underground mining. *Version B of Vietnam Journal of Science and Technology*, *64*(10DB), 43-45. https://doi.org/10.31276/VJST.64(10DB).

9. Mutize, C., & Wang, R. J. (2013). *Performance comparison of induction motor and line start PM motor for cooling fan applications*, in *Proceedings of the 21st Southern African Universities Power Engineering Conference*. 2013: North-West University, Potchefstroom, South Africa, (p. 122-126).

10. Maraaba, L. S., Memon, A. M., Abido, M., & AlHems, L. M. (2021). An efficient acoustic-based diagnosis of inter-turn fault in interior mount LSPMSM. *Applied Acoustics*, *173*, 107661. https://doi.org/10.1016/j.apacoust.2020.107661.

11. Elistratova, V. (2015). *Optimal design of line-start permanent magnet synchronous motors of high efficiency*. Ecole Centrale de Lille.

12. Li, J., Song, J., & Cho, Y. (2010). High performance line start permanent magnet synchronous motor for pumping system. *2010 IEEE International Symposium on Industrial Electronics*, 1308-1313. IEEE. https://doi.org/10.1109/ISIE.2010.5637082.

13. Do, N., Le, T., & Ngo, X. (2022). Effect of Permanent Magnet Structure on The Performance of LSPMSM with a Power of 22 kW and 3000 rpm. *IOP Conference Series: Earth and Environmental Science*, *1111*(1), 012047. IOP Publishing. https://doi.org/10.1088/1755-1315/1111/1/012047.

14. Bo, D., & Bin, X. (2013). Recent research of 2-pole asynchronous start permanent magnet synchronous motors. *2013 International Conference on Electrical Machines and Systems (ICEMS)*, 1090-1092. IEEE. https://doi.org/10.1109/ICEMS.2013.6754406.

15. Le, T. A., Bui, D. H., & Do, N. Y. (2022). Studying effect of proposal permanent magnet configurations on starting speed curve and

phase current waveform of line start magnet synchronous motors 15 kw, 3.000 rpm in steady state. *The University of Danang – Journal of Science and Technology*, *20*(7), 8-12.
16. Ganesan, A.U., & Chokkalingam, L.N. (2019). Review on the evolution of technology advancements and applications of line-start synchronous machines. *IET electric power applications*, *13*(1), 1-16. https://doi.org/10.1049/iet-epa.2018.5283.
17. Mingardi, D., Bianchi, N., & Dai Prè, M. (2017). Geometry of line start synchronous motors suitable for various pole combinations. *IEEE Transactions on Industry Applications*, *53*(5), 4360-4367. https://doi.org/10.1109/TIA.2017.2702581.
18. Baka, S., Sashidhar, S., & Fernandes, B. (2018). Multi-barrier two-pole line-start synchronous reluctance motor with high saliency for a bore-well submersible pump. *2018 IEEE International Conference on Industrial Technology (ICIT)*, 475-480. https://doi.org/10.1109/ICIT.2018.8352223.
19. Maraaba, L.S., Al-Hamouz, Z.M., Milhem, A.S., & Twaha, S. (2019). Comprehensive parameters identification and dynamic model validation of interior-mount line-start permanent magnet synchronous motors. *Machines*, *7*(1), 4. https://doi.org/10.3390/machines7010004.
20. Chingale, G., & Ugale, R. (2014). Harmonic filter design for line start permanent magnet synchronous motor. *2014 International Conference on Advances in Electrical Engineering (ICAEE)*, 1-4. https://doi.org/10.1109/ICAEE.2014.6838503.
21. Qiu, H., Zhang, Y., Yang, C., & Yi, R. (2020). Rotor structure with double cage for improved synchronous capability of line-start permanent magnet synchronous motors. *Technical Electrodynamics/Tekhnichna Elektrodynamika*, (1). https://doi.org/10.15407/techned2020.01.040.
22. Ugale, R.T., & Chaudhari, B.N. (2020). Performance enhancement of line start permanent magnet synchronous motor with a special consequent pole rotor. *IEEE Transactions on Energy Conversion*, *36*(3), 1972-1982. https://doi.org/10.1109/TEC.2020.3038725.
23. Yan, B., Yang, Y., & Wang, X. (2020). Design of a large capacity line-start permanent magnet synchronous motor equipped with hybrid salient rotor. *IEEE Transactions on Industrial Electronics*, *68*(8), 6662-6671. https://doi.org/10.1109/TIE.2020.3008360.
24. Bala, M.J., Jana, C., Chowdhury, S.K., & Deb, N.K. (2022). Performance analysis of different rotor configuration of LSPMSM for Electric Vehicles. *2022 IEEE Calcutta Conference (CALCON)*, 223-227. IEEE. https://doi.org/10.1109/CALCON56258.2022.10060046.
25. Baka, S., Sashidhar, S., & Fernandes, B. (2018). Design and optimization of a two-pole line-start ferrite assisted synchronous reluctance motor. *2018 XIII International Conference on Electrical Machines (ICEM)*, 131-137. https://doi.org/10.1109/ICELMACH.2018.8507187.
26. Soreshjani, M.H., & Sadoughi, A. (2014). Conceptual comparison of line-start permanent magnet synchronous and induction machines for line-fed of different conditions. *Journal of World's Electrical Engineering Technology*, *3*(1).
27. Mahmoudi, A., Roshandel, E., Kahourzade, S., Vakilipoor, F., & Drake, S. (2024). Bond graph model of line-start permanent-magnet synchronous motors. E*lectrical Engineering, 106*, 1667-1681. https://doi.org/10.1007/s00202-022-01654-w.
28. Heim, J.W., & Vander Wal, R.L. (2023). NdFeB Permanent Magnet Uses, Projected Growth Rates and Nd Plus Dy Demands across End-Use Sectors through 2050: A Review. *Minerals*, *13*(10), 1274. https://doi.org/10.3390/min13101274.
29. Do, N.Y., & Ngo, X.C. (2022). Effects of Voltage Unbalance on Matrix Converter Induction Motor Drive. *International Conference on Engineering Research and Applications*, 468-476. Springer. https://doi.org/10.1007/978-3-031-22200-9_53.
30. Do, N.Y., & Ngo, X.C. (2022). Effect of harmonic components and load carrying factor on the operating mode of induction motor. *AIP Conference Proceedings*, *2534*(1). https://doi.org/10.1063/5.0105148.
31. Do, N.Y., & Ngo, X.C. (2021). Influence of Single-Phase Voltage Loss and Load Carrying Mode on Mine Drainage Pump Motor in Vietnam. *Inżynieria Mineralna*. https://doi.org/10.29227/IM-2021-02-31.
32. Thuy, T.B., Cuong, N.X., & Do Nhu, Y. (2023). Effect of Permanent Magnet Structure on Working Characteristics of LSPMSM 3000 rpm. *IOP Conference Series: Earth and Environmental Science*, *1275*(1), 012049. IOP Publishing. https://doi.org/10.1088/1755-1315/1275/1/012049.

Конфігурація ротора для покращення робочих характеристик СДПМЛП у гірничодобувній галузі

До Нху И[1], *Трінь Б'єн Туй*[1, 2], *Ле Ань Туан*[3], *Нго Сюан Куонг*[*4]

1 – Ханойський університет гірничої справи та геології, м. Ханой, Соціалістична Республіка В'єтнам
2 – В'єтнамсько-Корейський коледж Куанг Нінь, м. Ха Лонг, Соціалістична Республіка В'єтнам
3 – Ханойський університет промисловості, м. Ханой, Соціалістична Республіка В'єтнам
4 – Школа інженерії та технологій, Університет Хюе, м. Туа Тхієн Хюе, Соціалістична Республіка В'єтнам
* Автор-кореспондент e-mail: ngoxuancuong@hueuni.edu.vn

Мета. Аналіз конфігурації ротора синхронного двигуна з постійними магнітами лінійного пуску (СДПМЛП) при використанні 3-стрижневої конструкції магніту у двох варіантах: із розділювальним магнітним сталевим мостом і без нього. Результати цього дослідження дозволяють вибрати відповідну конфігурацію ротора для отримання найкращих пускових характеристик, струму, моменту й ККД. Таким чином, з'явиться можливість заміни високоефективних асинхронних двигунів СДПМЛП на низькоефективні асинхронні двигуни, що використовуються у системах вентиляції й перекачування води, для підвищення енергоефективності в гірничодобувній промисловості.

Методика. У роботі використані аналітичні методи й методи моделювання у програмному забезпеченні Ansys/Maxwell, а також проведені лабораторні випробування для визначення впливу конфігурації ротора на пускові характеристики, робочий струм, коливання крутного моменту та ефективність роботи СДПМЛП в умовах видобутку корисних копалин.

Результати. Модель СДПМЛП була побудована на основі асинхронного двигуна потужністю 15 кВт–3 000 об/хв із двома конфігураціями ротора: із розділювальним магнітним сталевим мостом і без нього. Результати дослідження показують, що коли конфігурація ротора не має розділювального магнітного сталевого моста, СДПМЛП досягає максимальної швидкості за 0,45 секунди, синхронної швидкості 3 000 об/хв приблизно за 0,75 секунди, коливання крутного моменту 23,1 %, коефіцієнту повного гармонійного спотворення струму 14,3 % та ККД 93,3 %. На відміну від цього, коли конструкція ротора має розділювальний магнітний сталевий міст, запуск двигуна є більш складним: синхронна швидкість досягається за 1,14 секунди, пусковий момент нижчий, загальний коефіцієнт повного гармонійного спотворення струму становить 16,1 %, а ККД – 92,5 %.

Наукова новизна. Дослідження конфігурацій ротора СДПМЛП на основі асинхронного двигуна 15 кВт–3 000 об/хв із роздільним магнітним сталевим мостом і без нього. Результати досліджень дозволяють підібрати відповідну конфігурацію ротора для отримання найкращих пускових характеристик, струму, крутного моменту та продуктивності.

Практична значимість. Результати досліджень є важливими науковими рекомендаціями при проєктуванні й виготовленні СДПМЛП для застосування в підземних гірничих виробках з метою підвищення ефективності використання електроенергії в гірничій галузі.

Ключові слова: *кінцево-елементний аналіз, асинхронний двигун, лінійний пуск, постійний магніт, конфігурація ротора*

The manuscript was submitted 13.02.24.